minerals

MDPI

Article

Genesis and Geological Significance of Permian Oilfield Water in the Western Periphery of the Mahu Sag, Junggar Basin, China

Jiasi Li [1], Shuncun Zhang [2], Jun Jin [3], Aimin Jin [1,*], Zhanghua Lou [1] and Rong Zhu [1,*]

[1] Ocean College, Zhejiang University, Zhoushan 316021, China; 12034074@zju.edu.cn (J.L.); iwr@zju.edu.cn (Z.L.)
[2] Northwest Institute of Eco-Environment and Resources, Chinese Academy of Sciences, Lanzhou 730000, China
[3] Research Institute of Experiment and Detection, PetroChina Xinjiang Oilfield Company, Karamay 834000, China
* Correspondence: aiminjin@163.com (A.J.); zhurong@zju.edu.cn (R.Z.)

Abstract: Oilfield water contains valuable geological information and plays an important role in petroliferous basins, being closely related to diagenesis, reservoir physical properties, and hydrocarbon preservation conditions. Here we present a case study of oilfield water in Permian formations in the western periphery of the Mahu Sag, Junggar Basin, China. The genesis of oilfield water and its application in oil exploration were investigated through the coupling of tectonic activity, paleoclimate, and water–rock interaction. Volcanic activity provided a rich source of ions, and a hot paleoclimate intensifies the evaporation and concentration of sedimentary water. Tectonic fractures offered channels for water exchange among formations. Water–rock reactions, marked by sodic feldspathization and calcium feldspar dissolution, had profound effects on the oilfield water type and reservoir properties. We established a link between oilfield water and favorable targets for oil exploration. In terms of vertical trends, the Jiamuhe and Upper and Lower Urho formations have strong sealing abilities for hydrocarbon preservation. In the horizontal dimension, areas with high total-dissolved-solid and $CaCl_2$ concentrations, low r_{Na}/r_{Cl}, $r_{SO_4} \times 100/r_{Cl}$, $(r_{HCO_3+CO_3})/r_{Ca}$, and r_{Mg}/r_{Ca} ratios are favorable for oil exploration.

Keywords: oilfield water; genesis; geological significance; Permian; Mahu Sag

check for updates

Citation: Li, J.; Zhang, S.; Jin, J.; Jin, A.; Lou, Z.; Zhu, R. Genesis and Geological Significance of Permian Oilfield Water in the Western Periphery of the Mahu Sag, Junggar Basin, China. *Minerals* **2023**, *13*, 1043. https://doi.org/10.3390/min13081043

Academic Editor: Alexander G. Sokol

Received: 21 June 2023
Revised: 28 July 2023
Accepted: 2 August 2023
Published: 6 August 2023

1. Introduction

Oilfield water contains geological information and is therefore important to petroleum geology research. The generation, migration, and accumulation of oil and gas are impossible without the participation of oilfield water. It can affect the thermal decomposition of kerogen and its discharge of saturate-enriched oil. Without water, the process mainly generates pyrobitumen [1–3]. After oil is formed, the oilfield water becomes an important carrier and driving force in petroleum migration. Research undertaken since the 1970s has confirmed that groundwater dynamics are closely related to hydrocarbon migration and accumulation [4,5]. Oilfield water may be derived from sedimentary, infiltrated, plutonic, and converted water; it is often a mixture of these four components, so its genetic mechanism is complex [6,7]. Many methods have been employed to study the formation and evolution of oilfield water, whose chemical characteristics are commonly used to elucidate its underlying geological significance. Such characteristics include ionic, trace-element and isotopic compositions, and water–rock interactions [8–10]. The formation, transformation, dissolution, and exchange of minerals during diagenesis are closely associated with oilfield water, and the analysis of water–rock interactions and diagenetic minerals provides insights into the evolution of oilfield water [11–14].

The western periphery of the Mahu Sag in the Junggar Basin, China, is an important oil and gas production area, with a main producing layer of Permian reservoirs. Hydrocarbon

reservoirs in this area have complex oil–water relationships. Many test wells have produced oil and water, with some producing mainly water with little petroleum. Assays of collected stratigraphic water samples indicate that the oilfield water is characterized by high salinity, a diversity of water types, and complex ionic compositions. The reservoirs in the study area have undergone complex diagenesis, including the dissolution of a variety of minerals [15]. It has been speculated that the evolution of the Permian reservoirs in the Mahu Sag may be closely related to oilfield water, but systematic research is lacking. Previous studies have described the basic geological characteristics of the hydrocarbon reservoir [16,17], its diagenesis [18], source rocks, and tectonic evolution [19–21], but studies of oilfield water have been limited, leaving a number of unresolved issues, as follows. First, attention to oilfield water is restricted by production demands. Prospectors often use more direct indicators to find high-quality oil-producing areas, such as the qualities of hydrocarbon source rocks and reservoirs, ignoring the important role of other geological fluids in the identification of oil and gas reservoirs. Second, the evolutionary mechanism of oilfield water is complex and impossible to resolve by merely describing its ionic compositions without studying the interaction(s) between water, rocks, and hydrocarbons.

This study explored the genesis and evolution of oilfield water to evaluate its underlying geological significance to petroleum. Based on data from previous studies of the western periphery of the Mahu Sag, we were able to establish links between tectonic setting, sedimentation, diagenesis, and oilfield water, and we integrated these data with production data obtained through a partnership with the Xinjiang Oilfield Exploration and Development Research Institute. Our aim was to verify the importance of oilfield water in identifying highly productive oil and gas reservoirs, thus providing a reference for oil and gas exploration in Permian reservoirs of the western periphery of the Mahu Sag.

2. Regional Geology

The Mahu Sag is located in the northwestern part of the Junggar Basin, near the Zaire and Hala'alat mountains. The study area is located on the western slope of the Mahu Sag and is characterized by low terrain, gentle topography, and a great depositional thickness (Figure 1a,b). The effective storage layers discovered so far have depths exceeding 6000 m [22]. It is bounded to the west by the Ke-Bai fault zone, to the southwest by the Zhongguai uplift, and to the southeast by the Mahu Sag. Two primary faults developed in the study area, one in the north and one in the south. The northern fault is the Dawazhuang strike-slip fault, while the southern fault is the east-dipping reverse fault of the Hong 3 well. There are also numerous secondary faults that have developed near the two primary fault zones. These faults not only have compression properties but also have northeast-directed shear properties and belong to the strike-slip and reverse structures developed under an oblique thrust system [23]. The Mahu Sag contains high-quality source rocks, and the Ke-Bai fault zone is at a relatively high tectonic level, so hydrocarbons generated in the Mahu Sag can migrate through the slope area to the fault zone. As a major transition zone for oil and gas migration, the western periphery provides a favorable environment for oil and gas accumulation [24].

Permian strata in the study area provide enhanced hydrocarbon generation and storage conditions and are divided into five formations in ascending stratigraphic order: Jiamuhe, Fengcheng, Xiazijie, Lower Urho, and Upper Urho formations. The Upper Urho Formation was deposited in a fan delta environment, with the main subfacies being the fan delta front, and the thickness is 0–1417 m. The dominant lithology is gray sandy conglomerate, and the composition of the interstitial material is mainly tuff and andesite debris [18]. The Lower Urho Formation was mainly deposited in a fan delta front setting, with a thickness ranging from 100 to 1450 m. The upper section comprises a set of thick brown mudstone; the middle section is a set of gray–green and brown sandy conglomerate; the bottom of the formation comprises interbedded muddy siltstone, sandy conglomerate, and pebbly sandstone. The Xiazijie Formation was deposited in a fan delta plain setting, with the main lithologies being mudstone, brown sandy mudstone, fine sandstone, poorly sorted sandstone, and sandy conglomerate. Its thickness is 850–1160 m. The Fengcheng Formation, which is a

fan delta sedimentary system that formed in a post-orogenic extensional setting, consists of clastic sediment, dolomite, and volcanic rock. The thickness ranges from 430 to 1700 m. The Jiamuhe Formation comprises alluvial fan deposits, with a thickness ranging from 400 to 1800 m. Reservoirs within this formation are developed mainly within the central area and margins of the alluvial fan, which is characterized by complex lithofacies and high heterogeneity. The main lithologies are variegated mudstone, sandy conglomerate, sandstone, tuff, basalt, and andesite (Figure 1c).

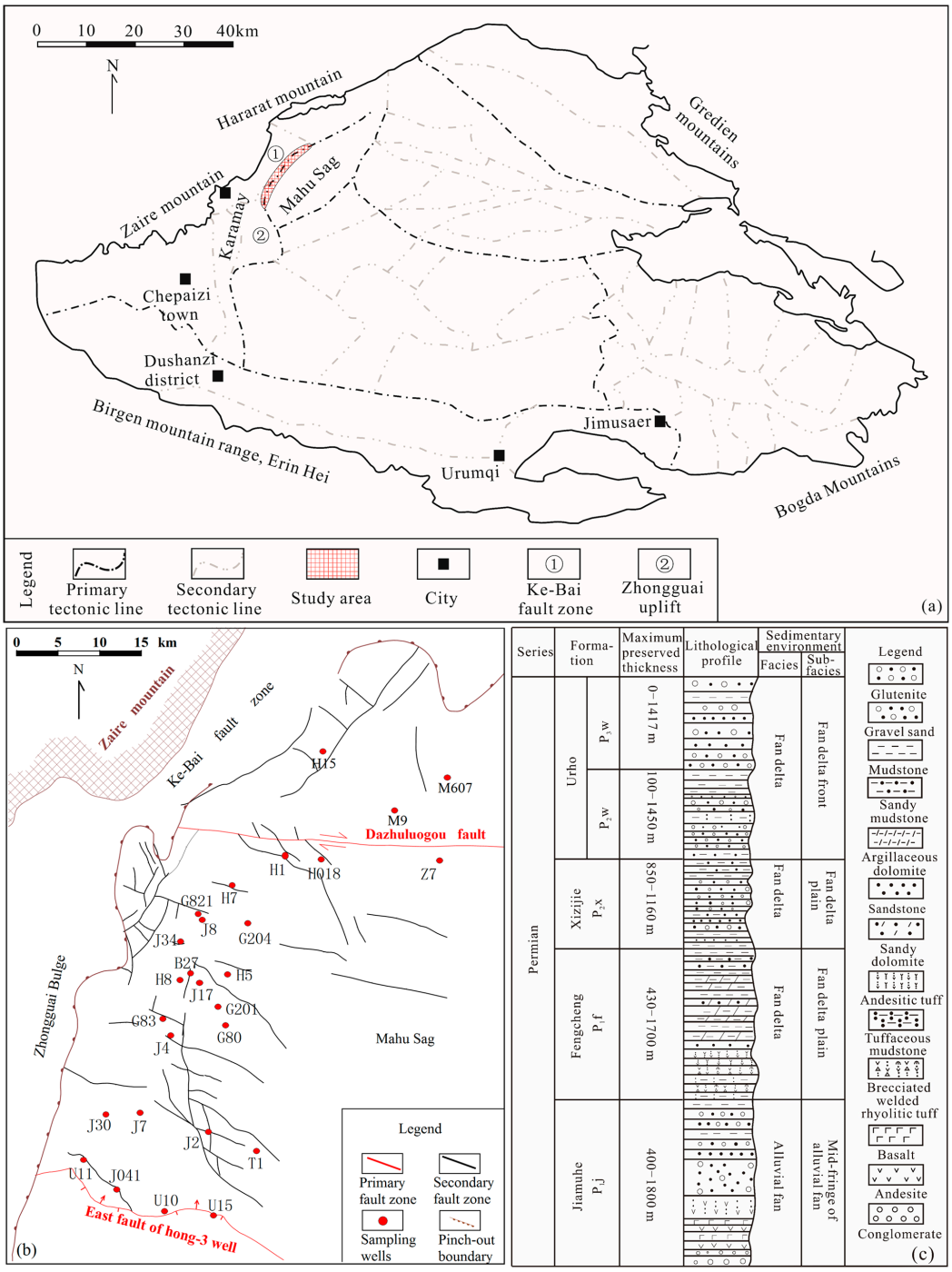

Figure 1. Geological setting of the western periphery of the Mahu Sag, Junggar Basin. (**a**) Location map of the study area; (**b**) well locations and structural features; and (**c**) stratigraphic log. In (**a**), the term "primary structural lines" and "secondary structural lines", respectively, refer to the boundaries of primary structural units and secondary structural units within a basin.

The Permian reservoirs at the western periphery of the Mahu Sag are located in the northwestern part of the Junggar Basin. They formed in a complex depositional environment and comprises a variety of rock types, suggesting that complex water–rock interactions occurred during their geological evolution. Water–rock interaction affects diagenesis, reservoir properties, and the chemical characteristics of oilfield water, further impacting the preservation of oil and gas. Therefore, studying the characteristics of oilfield water may provide insights into the processes of fluid evolution, thus facilitating the evaluation of reservoir quality and determining the relationship between oilfield water and hydrocarbon preservation conditions, and ultimately providing guidance for petroleum exploration.

3. Samples and Methods

Fifty-seven oilfield water samples were collected from Permian formations in the western periphery of the Mahu Sag: 16 from the Upper Urho Formation, 7 from the Lower Urho Formation, 7 from the Xiazijie Formation, 14 from the Fengcheng Formation, and 13 from the Jiamuhe Formation (Figure 1). All samples were taken during the early stage of drilling to ensure that they represented the original formation water and were not fracturing fluid or other drilling-related material.

Measurements of ion concentrations and mineralization in oilfield water were made according to Chinese trade standard SY/T 5523-2016 [25]. EDTA complexometry was used to determine Ca^{2+}, Mg^{2+}, and $SO_4{}^{2-}$ contents; the $AgNO_3$ titration method was used to determine Cl^- contents; acid–base titrations were used to determine $HCO_3{}^-$ and $CO_3{}^{2-}$ contents. The $(Na^+ + K^+)$ content was determined as follows:

$$(Na^+ + K^+)\ (meq) = \sum E_a - (Ca^{2+} + Mg^{2+})\ (meq) \quad (1)$$

$$(Na^+ + K^+)\ (mg\ L^{-1}) = 25(Na^+ + K^+)\ (meq\ L^{-1}) \quad (2)$$

where $\sum E_a$ is the sum of the milligram equivalent of anions.

X-ray diffraction data were used to determine the main mineral compositions of the strata in the study area. Thin sections from nine exploratory wells were analyzed using scanning electron microscopy (SEM) to identify the types and characteristics of diagenetic minerals. Production data from 24 wells were used to verify the reliability of results. Sampling and analyses were undertaken by the Xinjiang Oilfield Exploration and Development Research Institute.

4. Results

4.1. Total Dissolved Solids

TDS concentration refers to the number of inorganic ions per unit volume of oilfield water and is an important indicator of reservoir preservation conditions. There are eight major ions in Permian oilfield water of the western periphery, with a concentration order of $Cl^- > Na^+ + K^+ > CO_3{}^{2-} > HCO_3{}^- > Ca^{2+} > SO_4{}^{2-} > Mg^{2+}$. Ion concentrations are markedly higher than average values in river water. $(Na^+ + K^+)$ concentrations were 0.83–95.91 g L^{-1} with an average of 11.14 g L^{-1}, similar to the average value of modern seawater. Ca^{2+} concentrations ranged from below the detection limit to 9.46 g L^{-1} with an average of 1.60 g L^{-1}, which is notably higher than the modern seawater value. Mg^{2+} concentrations were the lowest of the positive ions in oilfield water, with an average of 0.02 g L^{-1} (lower than modern seawater). Cl^- had the highest anion concentrations of 0.21–58.39 g L^{-1} with an average of 12.61 g L^{-1}, which was lower than the average value for modern seawater. $CO_3{}^{2-}$ concentrations ranged from being undetectable to 68.35 g L^{-1} with an average of 7.55 g L^{-1}, much higher than that of modern seawater. $HCO_3{}^-$ concentrations were 0.07–47.99 g L^{-1} with an average of 4.56 g L^{-1}, again much higher than that of modern seawater. $SO_4{}^{2-}$ concentrations were the lowest of the studied anions with an average of 0.71 g L^{-1}, lower than that of modern seawater (Table 1). The

ionic composition of the oilfield water indicates that complex water–rock reactions took place in the Permian strata. Many ions enter oilfield water during diagenesis, and they have major impacts on the composition and properties of oilfield water (Table 1).

Table 1. Ionic compositions of Permian oilfield water in the western periphery of the Mahu Sag.

Types	g L^{-1}			Current Seawater [26] g L^{-1}	Current River [26] g L^{-1}
	Max	Min	Avg		
$K^+ + Na^+$	95.91	0.83	11.14	11.04	0.006
Ca^{2+}	9.46	0.00	1.60	0.42	0.015
Mg^{2+}	0.17	0.00	0.02	1.32	0.004
HCO_3^-	47.99	0.07	4.56	0.14	0.059
SO_4^{2-}	5.51	0.00	0.71	2.69	0.011
Cl^-	58.39	1.21	12.61	19.32	0.003
CO_3^{2-}	68.35	0.00	7.55	0.15	0.059
TDS	241.18	2.84	40.91	35.00	0.098

The TDS concentrations of oilfield water are often high under good storage conditions, whereas they are low under poor storage conditions [27,28]. In the western periphery of the Mahu Sag, the measured TDS concentrations of Permian oilfield water are 2.84–40.91 g L^{-1}, with some higher outliers of up to 241 g L^{-1}, much higher than the concentration of 35 g L^{-1} in average seawater (Table 1). The standard deviation of the TDS data set is 69.79 g L^{-1}, indicating a high level of dispersion in the data. Some water samples have TDS values that are significantly higher than the overall data set. This could be attributed to the following factors: ① Geological factors: There may be geological formations or rocks with high mineralization, leading to abnormally high TDS levels in the water samples. ② Water source mixing: The water samples could be a mixture of water from different sources, some of which may have higher mineralization, resulting in an overall increase in TDS levels. ③ Saltwater intrusion: Saltwater intrusion may occur in the underground water of the oil field, where water with high salt concentration enters the oil field water system, causing abnormally high TDS levels in the water samples [29,30]. Generally, these data are reliable and can reflect some geological information, provided that there is no human interference.

($Na^+ + K^+$) and Cl^- concentrations in the Jiamuhe and Upper and Lower Urho formations are strongly correlated with TDS concentrations (Figure 2a,b), indicating that oilfield water was strongly influenced by evaporation. The correlation between Cl^- and TDS concentrations in the Fengcheng and Xiazijie formations is relatively weak, indicating that less evaporation occurred during the deposition of the Fengcheng and Xiazijie formations. The TDS concentrations show a peak at 4000–4500 m depth in the studied formations (Figure 3a). Within this depth range, ($Na^+ + K^+$), HCO_3^-, and Cl^- concentrations also peak, indicating active water–rock reactions within these formations (Figure 3b–e).

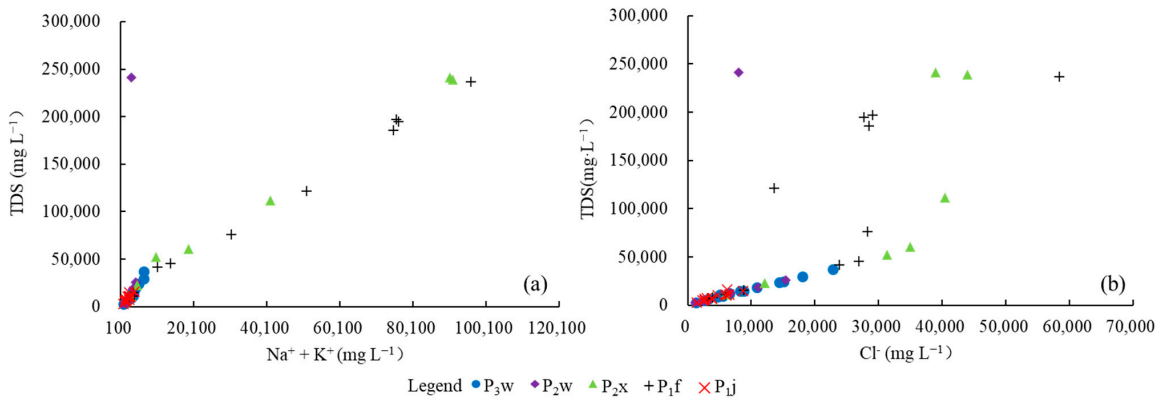

Figure 2. Relationship between TDS concentrations and ($Na^+ + K^+$) and Cl^- concentrations. P_3w: Upper Urho formation; P_2w: Lower Urho formation; P_2x: Xiazijie formation; P_1f: Fengcheng formation; P_1j: Jiamuhe formation.

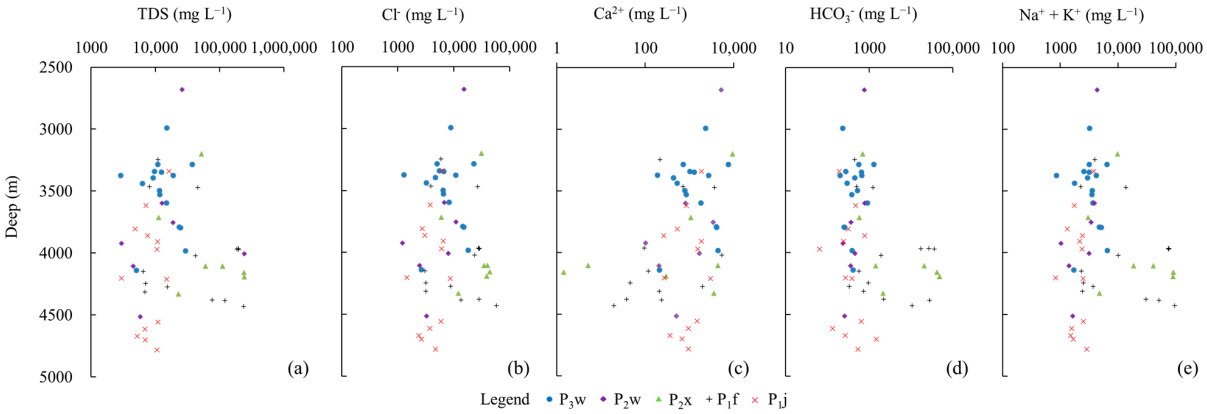

Figure 3. Variations in the chemical characteristics of oilfield water with depth for (**a**) TDS; (**b**) Cl^-; (**c**) Ca^{2+}; (**d**) $HCO_3{}^-$; and (**e**) (Na^+ + K^+).

4.2. Oilfield Water Type

Oilfield water type is an important parameter in the determination of oil and gas preservation conditions. Here, the Surin classification method [31] was used to classify water types and to identify reservoir sealing properties and hydrocarbon preservation conditions. This method applies the content ratio of major ions in oilfield water as a classification criterion, using the r_{Na}/r_{Cl}, $r_{Na-Cl}/2r_{SO_4}$, and $r_{Cl-Na}/2r_{Mg}$ ratios as classification coefficients, and divides the oilfield water into four types: sodium bicarbonate ($NaHCO_3$)-type and sodium sulfate (Na_2SO_4)-type water in a continental environment, magnesium chloride ($MgCl_2$)-type water in a marine environment, and calcium chloride ($CaCl_2$)-type water in a deep burial environment (Table 2). The Surin classification method is widely used for its rationality and simplicity, and it is critical in the determination of oilfield water types, oil and gas preservation conditions, and hydrocarbon migration pathways.

Table 2. Relationships between water type and the classification coefficients of oil and gas fields.

Water Type	Classification Coefficient			Setting
	r_{Na}/r_{Cl}	$r_{Na-Cl}/2r_{SO_4}$	$r_{Cl-Na}/2r_{Mg}$	
$NaHCO_3$	>1	<1	<0	Continental environment
Na_2SO_4	>1	>1	<0	
$MgCl_2$	<1	<0	<1	Marine environment
$CaCl_2$	<1	<0	>1	Deep burial environment

Permian oilfield water in the western periphery of the Mahu Sag is primarily of the $CaCl_2$ type, which accounts for 72% of the samples; $NaHCO_3$-type water accounts for 25% of the samples, and the Na_2SO_4-type accounts for 3% (Table 3). The formation of $CaCl_2$-type water requires a relatively closed environment with good sealing of the roof and interlayers of the reservoir. The oil, gas, and water system have been located in the hydrogeological blocking zone or stagnant zone for a long time, which can reduce the degradation to the oil and gas reservoir and is conducive to the preservation of oil and gas. $NaHCO_3$-type formation water is generated in a relatively open environment, with poor sealing; consequently, oil and gas reservoirs are vulnerable to degradation, which is not conducive to the accumulation and preservation of oil and gas. Both the $CaCl_2$ and Na_2SO_4 types occur in the Upper Urho Formation, with the $CaCl_2$ type predominating, indicating that the formation is well sealed. Oilfield water in the Lower Urho Formation is mainly of the $CaCl_2$ type, with scarce $NaHCO_3$-type water, indicating that the formation has suitable sealing properties and good preservation conditions. The Xiazijie Formation water is mainly of the $CaCl_2$ and $NaHCO_3$ types, with the $NaHCO_3$ type being dominant, suggesting more active oilfield water and poorer sealing and preservation conditions. The Fengcheng

Formation contains three water types ($NaHCO_3$, $CaCl_2$, and Na_2SO_4), with the $NaHCO_3$ type predominating, indicating poor sealing qualities and high-activity water, meaning the conditions are not favorable for oil and gas preservation. The Jiamuhe Formation contains $CaCl_2$-type water, indicating good preservation conditions. This succession of changes of the water types is influenced by water–rock interactions, as discussed below.

Table 3. Oilfield water types in Permian strata of the western periphery of the Mahu Sag.

Type	Concentration/Unit					Total	Hydrogeological Interpretation
	P_3w	P_2w	P_2x	P_1f	P_1j		
$NaHCO_3$	-	1	3	9	1	14	Hydrogeological active area, which has a destructive effect on oil and gas
$CaCl_2$	15	6	4	4	12	41	The formation has good sealing properties, which are favorable for oil and gas preservation
Na_2SO_4	1	-	-	1	-	2	Affected by surface water; the formation has poor oil and gas preservation potential

4.3. Chemical Parameters of Oilfield Water

Chemical parameter analysis can reveal important information about the geochemical conditions of oilfield water and the intensity of fluid–rock interactions. This information is more informative than simply identifying the type of oilfield water. By studying the relationship between oilfield water and oil and gas migration and accumulation, chemical parameter analysis can aid in predicting the location and properties of oil and gas reservoirs.

4.3.1. Na^+ and Cl^-

The r_{Na}/r_{Cl} ratio reflects the degree of concentration and activity level of oilfield water, and the reservoir sealing properties and preservation potential. Ratios of >0.87 indicate that the oilfield water has been affected by external factors and is not favorable for oil and gas preservation. The higher the ratio, the more pronounced the influence of infiltration water, and the more unfavorable the reservoir for hydrocarbon preservation. Ratios of <0.87 indicate better reservoir sealing properties, which are beneficial to hydrocarbon accumulation [12]. In the western periphery, the r_{Na}/r_{Cl} ratio of Permian oilfield water varies widely, with minimum, maximum, and average values of 0.44, 2.43, and 0.92, respectively. Ranges (averages) for the different formations are as follows: Upper Urho Formation, 0.5–1.02 (0.78); Lower Urho Formation, 0.44–1.31 (0.77); Xiazijie Formation, 0.48–2.43 (1.05); Fengcheng Formation, 0.65–2.15 (1.22); and Jiamuhe Formation, 0.44–1.22 (0.79) (Figure 4a).

4.3.2. SO_4^{2-} and rCl^-

In relation to interactions between oilfield water and hydrocarbons that consume sulfate, the $r_{SO_4} \times 100/r_{Cl}$ ratio provides a measure of the consumption of sulfate and is an indicator of oilfield water redox conditions. With high sulfate removal, the ratio is near zero, indicating better sealing, a reducing environment, active water–rock interaction, and good hydrocarbon preservation conditions [32]. The values for Permian oilfield water of the present study ranges between zero and 23.55 with an average of 2.93, indicating that the reservoir has suitable sealing properties and relatively intense reduction, which are beneficial to oil and gas preservation. However, the ratio varies markedly between formations. Ranges (averages) for the different formations are as follows: Upper Urho Formation, 0.04–9.23 (2.0); Lower Urho Formation, 0–9.28 (1.94); Xiazijie Formation, 0.08–3.56 (1.46); Fengcheng Formation, 0.13–7.64 (2.60); and Jiamuhe Formation, 0.27–23.55 (5.74) (Figure 4b).

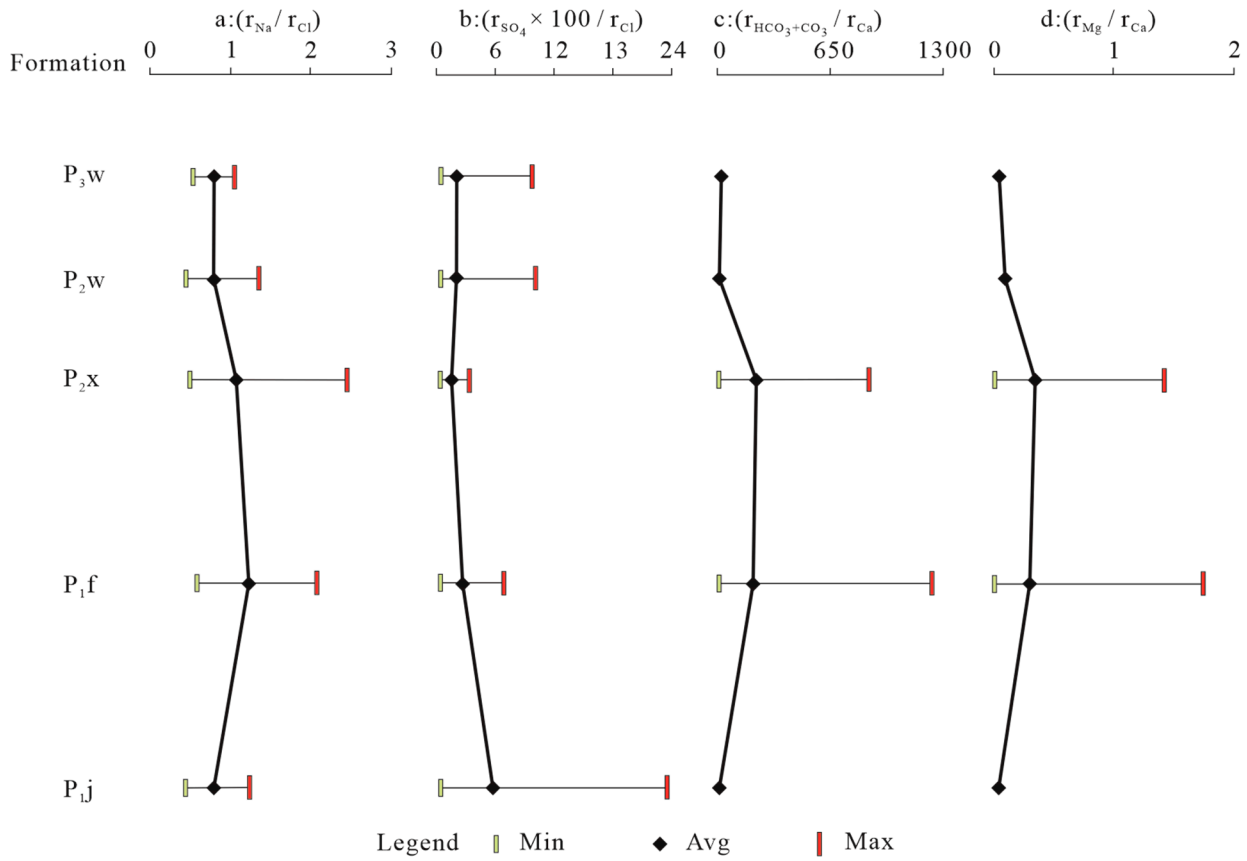

Figure 4. Vertical profiles of chemical parameters for Permian oilfield water in the western periphery of the Mahu Sag, including (**a**) r_{Na}/r_{Cl}, (**b**) $r_{SO_4} \times 100/r_{Cl}$, (**c**) $(r_{HCO_3+CO_3})/r_{Ca}$, and (**d**) r_{Mg}/r_{Ca}.

4.3.3. $(HCO_3^- + CO_3^{2-})$ and Ca^{2+}

The $(r_{HCO_3+CO_3})/r_{Ca}$ ratio reflects oilfield water decarbonization and hydrocarbon preservation conditions. Previous studies have shown that lower ratios indicate oilfield water close to the regional hydrodynamic stagnation zone, where water usually has strong decarbonization action and the reservoir is more favorable for oil and gas preservation [33,34]. The values for Permian formations in the western periphery are generally in the range of 0.04–1240, with an average of 66.49. Ranges (averages) for the different formations are as follows: Upper Urho Formation, 0.04–1.27 (0.39); Lower Urho Formation, 0.07–2.58 (0.72); Xiazijie Formation, 0.05–820.72 (215.27); Fengcheng Formation, 0.11–1240.65 (195.56); and Jiamuhe Formation, 0.07–2.29 (0.54) (Figure 4c). Overall, reservoirs of the Jiamuhe and Upper and Lower Urho formations have relatively good oil and gas preservation conditions.

4.3.4. Mg^{2+} and Ca^{2+}

The r_{Mg}/r_{Ca} ratio reflects the degree of secondary pore development; the lower the ratio, the more developed the secondary pores [35]. The value of this ratio in the study area is generally low, ranging from 0 to 1.75, with an average of 0.14, indicating that secondary pores are well-developed in the Permian reservoirs. Ranges (averages) for the different formations are as follows: Upper Urho Formation, 0–0.13 (0.04); Lower Urho Formation, 0–0.35 (0.09); Xiazijie Formation, 0–1.45 (0.35); Fengcheng Formation, 0–1.75 (0.3); and Jiamuhe Formation, 0–0.15 (0.04) (Figure 4d).

5. Discussion

5.1. Oil and Gas Preservation

The chemical parameters of oilfield water, as described above, provide clues to the quality of different reservoirs. Here we discuss the correlations between different hydrochemical parameters, and further investigate variations in physical properties and hydrocarbon preservation conditions in Permian reservoirs.

The relationship between r_{Na}/r_{Cl} and $r_{SO_4} \times 100/r_{Cl}$ for oilfield water can be used to divide the preservation environment into transition, preservation, non-preservation, and weak preservation zones, which reflect the hydrocarbon preservation conditions [36]. The data of the Upper Urho, Lower Urho, Xiazijie, and Jiamuhe formations are mainly in the preservation zone. The Fengcheng Formation has two data points in the transition and non-preservation zones (Figure 5). This indicates that preservation conditions in the Upper Urho, Lower Urho, Xiazijie, and Jiamuhe formations are more favorable for hydrocarbon preservation than those of the Fengcheng Formation.

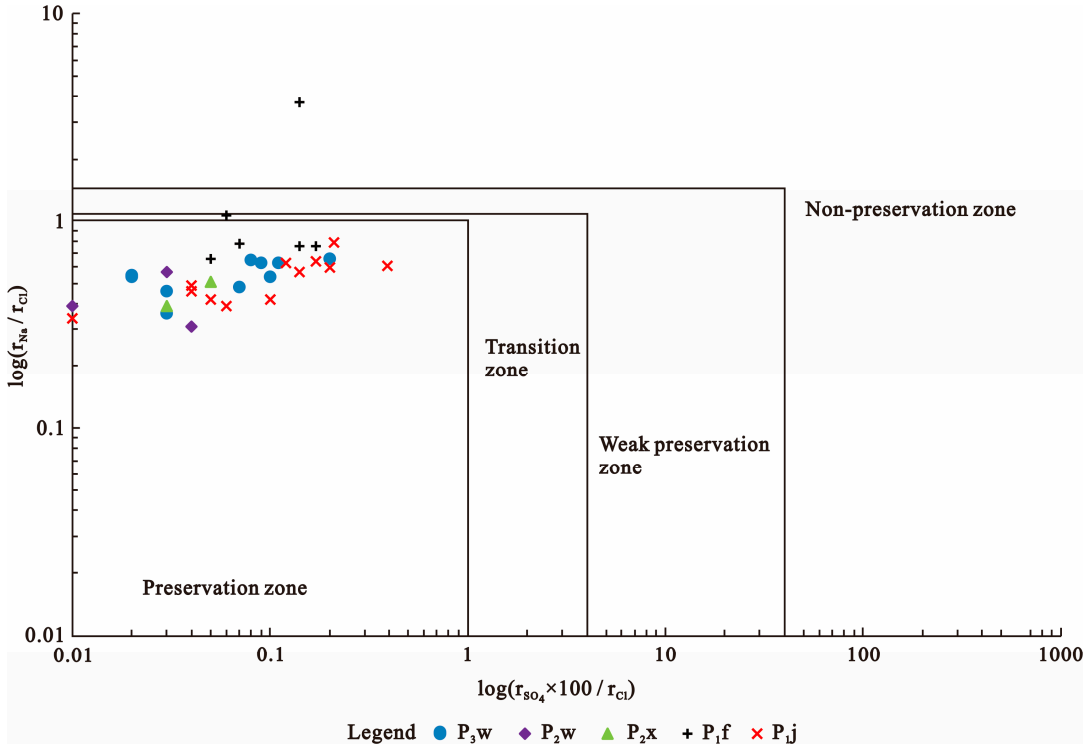

Figure 5. Classification of Permian oilfield water–oil and gas preservation conditions in the western periphery of the Mahu Sag.

The oilfield water of the Upper and Lower Urho formations has similar chemical characteristics, with low values of r_{Na}/r_{Cl}, $r_{SO_4} \times 100/r_{Cl}$, $(r_{HCO_3+CO_3})/r_{Ca}$, and r_{Mg}/r_{Ca}, indicating that the oilfield water has undergone a high degree of concentration, with weak desulfurization and decarbonization effects. The reservoir is near the regional hydrodynamic stagnation zone, with good sealing and secondary pores. These factors provide good conditions for oil and gas preservation. The Xiazijie and Fengcheng formations have lower $r_{SO_4} \times 100/r_{Cl}$ ratios, but higher r_{Na}/r_{Cl}, $(r_{HCO_3+CO_3})/r_{Ca}$, and r_{Mg}/r_{Ca} ratios than the Upper and Lower Urho formations, indicating that as their secondary pore content decreases, the degree of concentration of oilfield water decreases, with a deterioration in reservoir sealing and oil and gas preservation conditions. Compared with the other formations, the Jiamuhe Formation has higher $r_{SO_4} \times 100/r_{Cl}$ ratios and lower $(r_{HCO_3+CO_3})/r_{Ca}$ and r_{Mg}/r_{Ca} ratios. In this formation, oilfield water undergoes intense concentration and

reduction. The reservoir is near the stagnant groundwater zone, secondary pores are relatively well-developed, and the sealing is conducive to hydrocarbon preservation.

5.2. Genesis of Oilfield Water

5.2.1. Tectonic Activity and Paleoclimate

The contents of ions and TDS in oilfield water are closely related to paleo-sedimentary chemistry. Those of Permian oilfield water in the western periphery indicate that water in the study area is rich in alkali and alkaline–earth metal ions. The sedimentary and tectonic setting of the study area indicates that the Mahu Sag is a Carboniferous–Quaternary depression that formed on pre-Carboniferous folded basement. It has thus undergone a complex tectonic evolution. From the Permian to Triassic, the Mahu Sag was dominated by sedimentary filling. The main evolutionary event involved long-term post-orogenic extension during the late Carboniferous to early Permian. Compression and thrusting occurred during the middle Permian to Middle Triassic, forming an intracratonic depression by the Late Triassic. The formation of the depression involved various sedimentary systems, including alluvial fans, fan deltas, and lake facies [37–39]. Two sets of source rocks were formed during the Permian, namely the Jiamuhe and Fengcheng formations. The period of their deposition was marked by basic volcanism [40], with volcanic materials entering the reservoirs, such as alkali (Na^+, K^+) and alkaline–earth (Ca^{2+}) metal ions, which provided a basis for alkali-containing mineral generation in the reservoirs. Such minerals are an important component of oilfield water and influence its properties.

The paleoclimate of the Mahu Sag was arid, with high rates of evaporation. Such a climate promoted the alkalinization of water and the formation of alkaline lake environments [24,37–39]. The relationships between ion types and TDS in oilfield water indicate that the characteristics of oilfield water in the Jiamuhe, and Lower and Upper Urho formations were obviously influenced by evaporation (Figure 2). Strong evaporation causes a remarkable concentration of oilfield water, and interlayers of mudstone and tuffaceous mudstone create a closed environment that is beneficial to the preservation of oilfield water [41]. Therefore, the oilfield water of Jiamuhe and Lower and Upper Urho formations has high concentrations of TDS. The Jiamuhe and Upper and Lower Urho formations have r_{Na}/r_{Cl} ratios << 0.85, indicating that oilfield water underwent relatively high cation exchange and adsorption.

The depositional environment in the Fengcheng and Xiazijie formations changed as a result of deep hydrothermal and tectonic activity, with the lake basin becoming highly saline and occlusive [17,42]. During this period, volcanic and tectonic activity were pronounced, forming a series of fault zones on the northwestern margin of the Junggar Basin [43]. Volcanism provided Na, Mg, Ca, and other elements for alkali-containing minerals. Large, deep faults provided channels for hydrothermal migration, and alkaline minerals of the soda group, rich in Na_2O and CO_2, were accumulated in the strata. Such minerals are soluble in water and hydrolyze to release Na^+ ions and CO_2 gas during early diagenesis. This environment was conducive to the generation of $NaHCO_3$-type water. Furthermore, large volumes of volcanic material in the Jiamuhe Formation were transported along faults within hydrothermal fluid, affecting the composition of the Fengcheng and Xiazijie formations fluids. Oilfield water of the Fengcheng and Xiazijie formations is thus characterized by high TDS concentrations (Figure 3a) and is minimally relevant to the content of Cl^- (Figure 2b).

5.2.2. Water–Rock Interactions

The sources and compositions of oilfield water are closely related to water–rock interactions, with different reaction products resulting in different chemical properties for the water. Davisson et al. (1996) proposed a method of describing fluid–rock interactions based on the relationship between the depletion of Na^+ and the enrichment of Ca^{2+} relative to seawater, using a $Na_{deficit}$–Ca_{excess} diagram [7,44,45]. The $Na_{deficit}$–Ca_{excess} relationship of the Permian oilfield water in the present study area is discussed here in terms of this

method. The $Na_{deficit}$–Ca_{excess} diagram (Figure 6) indicates that, compared with seawater, the oilfield water of the Jiamuhe and Upper and Lower Urho formations is notably depleted in Na^+ and enriched in Ca^{2+}. The data plot on the Basin Fluid Line (BFL) indicates that the reservoirs underwent Na and Ca ion-replacement reactions [33,46] (Figure 6a–c). SEM observations indicate that the main minerals present in the Permian reservoirs are quartz, plagioclase, laumontite, heulandite, and microcline (as shown in Figure 7). Furthermore, it was observed that albite, a type of plagioclase, was dissolved. (Figure 8h,i). These lines of evidence indicate that water–rock reactions of albite and Ca occurred in the Jiamuhe and Upper and Lower Urho formations as follows:

$$CaAl_2Si_2O_8 + 4SiO_2 + 2Na^+ = 2NaAlSiO_8 + Ca^{2+} \quad (3)$$

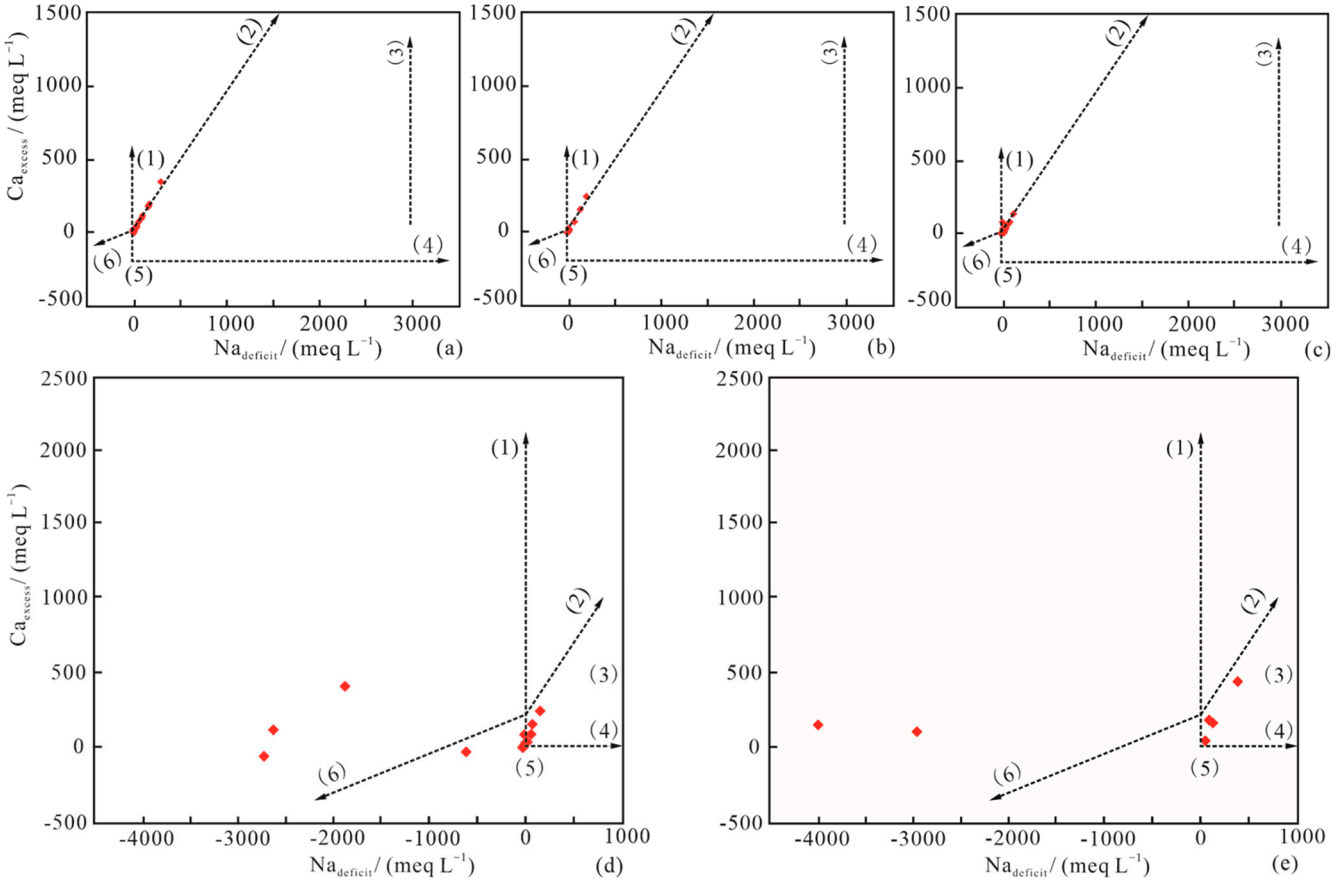

Figure 6. $Na_{deficit}$–Ca_{excess} plots for the western periphery of the Mahu Sag, showing the dissolution of $CaSO_4$ and dolomitization (1); exchange reactions between one Ca and two Na ions (2); a reaction mixture (3); ocean evaporation (4); saturated salt rock (5); and dissolution of salt rock (6). (**a**) Upper Urho Formation; (**b**) Lower Urho Formation; (**c**) Jiamuhe Formation; (**d**) Fengcheng Formation; (**e**) Xiazijie Formation.

The ionic contents of the Fengcheng and Xiazijie formations were much higher than those of the other formations (Figure 3b–e), and the enrichment of Ca^{2+} relative to seawater was not obvious in the former. About 50% of the samples show obvious Na^+ enrichment relative to seawater, indicating the dissolution of salt rock (Figure 6d). Similarly, most samples of the Xiazijie Formation plot were near the Basinal Fluid Line, with some samples showing Na^+ enrichment relative to seawater, indicating sodic feldspathization of Ca feldspars accompanying the dissolution of salt rock (Figure 6e). The Fengcheng and

Xiazijie formations are rich in carbonate minerals, especially dolomite and calcite (Figure 7). Carbonate rocks dissolve in an acidic fluid environment as follows:

$$CaCO_3 + H^+ = Ca^{2+} + HCO_3^- \quad (4)$$

$$CaMgCO_3 + H^+ = Ca^{2+} + Mg^{2+} + HCO_3^- \quad (5)$$

The dissolution of carbonate rocks was thus a major source of oilfield water in the Fengcheng and Xiazijie formations. Sandy and argillaceous dolomites that are rich in carbonate components are significant targets of dissolution (Figure 1c).

Oilfield water of the Fengcheng and Xiazijie formations is mainly of the $NaHCO_3$ type, with high TDS contents. Previous studies [27] have reported that $NaHCO_3$-type water is relatively rare in petroliferous basins and is often related to the migration of CO_2 from mantle sources or migration of oil and gas along basement faults [47,48]. The Fengcheng Formation is the main Permian hydrocarbon source rock in the study area, and large volumes of CO_2 would have been produced during the maturation of organic matter. CO_2 dissolves in oilfield water, raising the HCO_3^- concentration and promoting the generation of $NaHCO_3$-type water with high TDS contents. The r_{Na}/r_{Cl} and $(r_{HCO_3+CO_3})/r_{Ca}$ ratios of the Fengcheng and Xiazijie formations are relatively high (Figure 4a–c), indicating relatively strong oilfield water activity. In addition, volcanism occurred during the deposition of the Fengcheng Formation, and the Wuxia Kebai fault zone continued to expand. Under the influence of formation pressure, the active oilfield water of the Fengcheng Formation mixed with oilfield water of the Xiazijie Formation along these faults; the latter water inherited features of the former, evolving to $NaHCO_3$-type water with a high TDS content. Oilfield water in the Fengcheng Formation was thus influenced by the dissolution of carbonate rocks and the expulsion of hydrocarbons from source rocks. The genesis of oilfield water in the Xiazijie Formation was more complex and was influenced by salt rock dissolution, sodic feldspathization of Ca feldspars, and the complex Permian fault system.

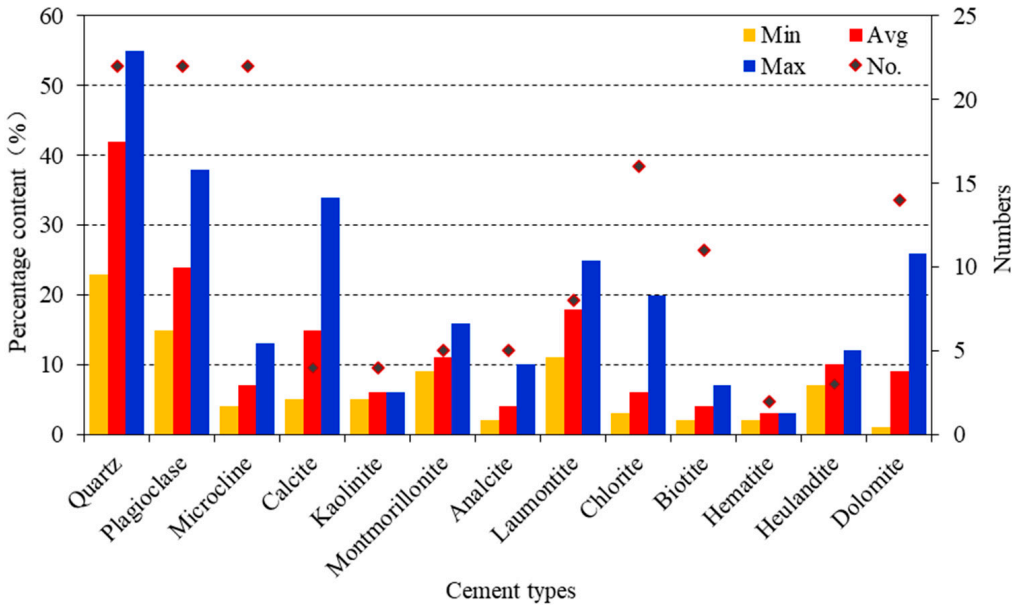

Figure 7. Types of interstitial material in Permian reservoirs in the western periphery of the Mahu Sag.

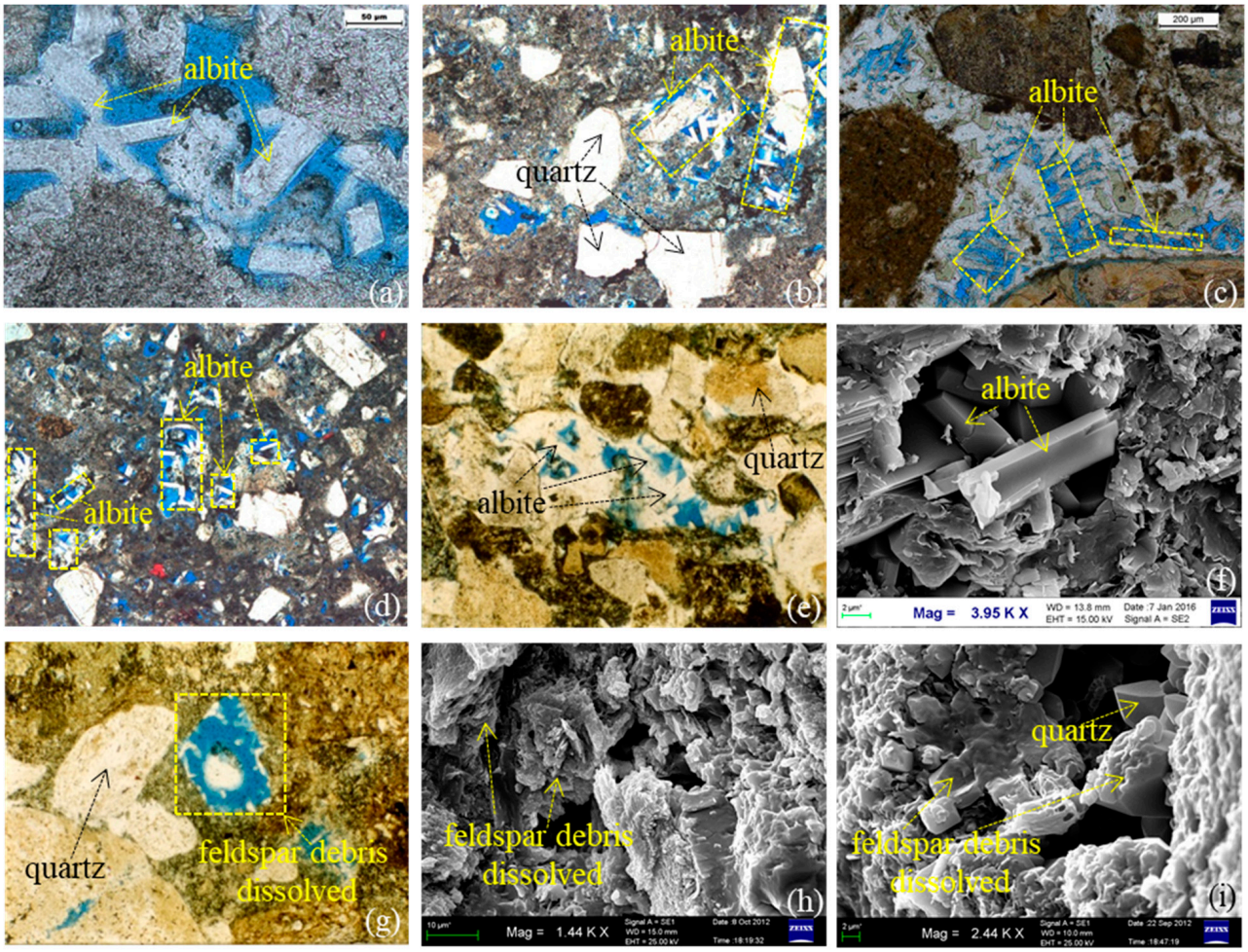

Figure 8. Microscopic characteristics of feldspar in the Permian reservoir of the western periphery of the Mahu Sag. (**a**) Well YT1, 4872.5 m, P_2w; intergranular pores of sandy conglomerate are filled with authigenic albite; the albite crystal is intact with no dissolution; ×50. (**b**) Well JL31, 3149.41 m, P_1j; matrix contains tuffaceous, intergranular pores; dissolution pores developed in the matrix; pores are filled with columnar authigenic albite; ×50. (**c**) Well YB4, 3870.11 m, P_2w; euhedral columnar albite is developed in intergranular pores of sandy conglomerate; ×50. (**d**) Well JL31well, 3149.86 m, P_1j; authigenic albite is developed in the matrix; dissolution pores are rich in tuffaceous sandstone; albite formed after the dissolution; ×50. (**e**) Well K80, 4156.77 m, P_2w; residual intergranular pores of sandstone are filled with authigenic albite minerals and intercrystalline pores are developed; ×80. (**f**) Well YB4, 3915.31 m, P_2w; columnar albite has grown in intergranular dissolution pores; minerals have well-developed crystal forms without dissolution; ×3950 (SEM). (**g**) Well K80, 4155.23 m, P_2w; feldspar particles in sandstone are dissolved to form moldic pores and intragranular dissolution pores (intra-feldspar pores); ×80. (**h**) Well J206, 4012.62 m, P_3w; feldspar particles are strongly corroded, producing a large number of dissolution pores in the particles; ×1440 (SEM). (**i**) Well JL8 well, 3290.35 m, P_3w; clastic feldspar particles have undergone strong dissolution, and authigenic quartz has grown in the intergranular dissolution pores; ×2440 (SEM).

6. Geological Significance

6.1. Physical Properties of Reservoirs

Secondary pores in Permian reservoirs in the western periphery of the Mahu Sag are well-developed, and albite dissolution is an important contributor to pore formation [49,50], as indicated by the characteristic rMg^{2+}/rCa^{2+} ratios of oilfield water (Figure 4d). The dissolution of feldspar debris particles is prevalent in the study area, whereas feldspar cement seldom dissolves. In thin sections, albite cement filling intergranular pores comprises short

columnar crystals that have not been dissolved (Figure 8a–e). Further examination by SEM revealed that feldspar of the cement has a well-developed crystal form and has not been subjected to dissolution (Figure 8f); instead, it is the feldspar debris particles that dissolve. The thin section and SEM analyses show that feldspar debris particles dissolve readily, forming moldic and dissolution pores (Figure 8g–i). The main dissolution products are kaolinite and quartz, and according to the different types of feldspar, there are three main dissolution reactions:

$$2KAlSi_3O_8 \text{ (K-feldspar)} + 2H^+ + H_2O = Al_2Si_2O_5(OH)_4 \text{ (kaolinite)} + 4SiO_2 \text{ (quartz)} + 2K^+ \quad (6)$$

$$2NaAlSi_3O_8 \text{ (albite)} + 2H^+ + H_2O = Al_2Si_2O_5(OH)_4 \text{ (kaolinite)} + 4SiO_2 \text{ (quartz)} + 2Na^+ \quad (7)$$

$$CaAl_2Si_2O_8 \text{ (anorthite)} + 2H^+ + H_2O = Al_2Si_2O_5(OH)_4 \text{ (kaolinite)} + Ca^{2+} \quad (8)$$

The dissolution of feldspar debris particles is a constructive diagenetic process, forming dissolution pores that can improve the reservoir's pore-permeability conditions. The precipitation and growth of authigenic quartz, on the other hand, is a destructive diagenetic process, as it occupies pore space, reducing porosity and permeability. In Figure 8, authigenic quartz particles can be clearly observed, with complete crystal forms. Most of the quartz has undergone authigenic enlargement without dissolution, filling the pore interiors and occupying some or all of the pore space (Figure 8b,e,g,i). The excessive growth of quartz in the study area is primarily a chemical reaction. On one hand, the dissolution of feldspar debris particles forms quartz crystals. On the other hand, as the concentration of silica-bearing fluids increases, under certain temperature and pressure conditions, dissolved silica in the fluids re-crystallizes to form quartz crystals. This recrystallization process occurs at the edges of previously formed quartz crystals, resulting in edge enlargement (Figure 8b,e).

Previous studies have shown obvious homoionic and salt effects in high-TDS oilfield water. Feldspar dissolves when the fluid environment becomes acidic. However, if there are high concentrations of Na^+ and Cl^- ions in the fluid, the exchange of Na^+ and Cl^- from feldspar to fluid is inhibited, and feldspar dissolution is impeded. This is termed the 'homoionic effect'. Aluminum silicate minerals dissolve more readily as the TDS concentration increases (i.e., the 'salt effect') [51]. The TDS content of Permian oilfield water in the study area is fairly high (Figure 3a), and alkali and alkaline–earth metal ion concentrations are high, especially Na^+ and K^+ in the Fengcheng and Xiazijie formations where they are notably higher than Ca^{2+} concentrations (Figure 3c–e). In this case, the homoionic effect is not conducive to the dissolution of albite or K-feldspar because these minerals are rich in alkali metal ions. The salt effect aids the dissolution of Ca feldspar because this mineral is rich in alkaline–earth metal ions [14,52,53]. Therefore, the dissolution of Ca feldspar is an important feature of diagenesis in the study area and can be used to assess the physical properties of reservoirs.

6.2. Favourable Areas for Exploration

Distribution maps (Figure 9) of TDS concentration, and r_{Na}/r_{Cl} and $r_{SO_4} \times 100/r_{Cl}$ ratios of the Upper Urho Formation were prepared to indicate the association between the chemical characteristics of oilfield water and areas suitable for exploration. The average porosity distribution of the Upper Urho Formation was used to discuss the relationship between the chemical characteristics of oilfield water and porosity. The influence of the sedimentary environment was also considered through source direction and facies distribution.

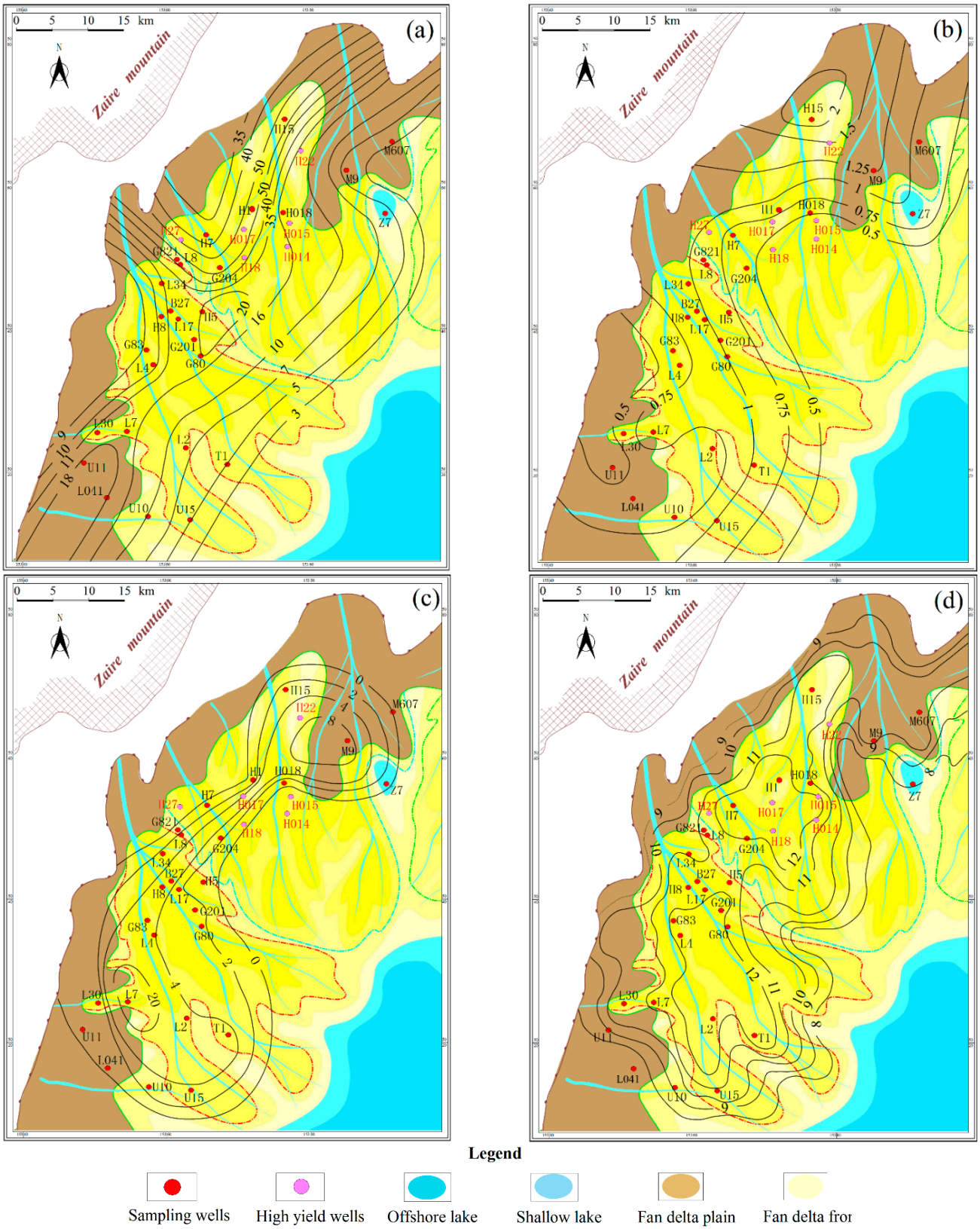

Figure 9. Distribution of oilfield water chemistry and average porosity for the Permian Upper Urho Formation in the western periphery of the Mahu Sag. The figure shows the distributions of (**a**) TDS concentration; (**b**) r_{Na}/r_{Cl} ratio; (**c**) $r_{SO_4} \times 100/r_{Cl}$ ratio; and (**d**) porosity.

Material sources are distributed in a northwesterly direction in the study area, with a fan delta plain, fan delta front, front fan delta, lakeside, and shallow lake developing from the slope area to the center of the depression. The Upper Urho Formation has the most widespread distribution of fan delta front subfacies. TDS is distributed in a banded pattern, with high-value areas to the west and north, and the low-value regions to the east and south. The high-value area is mainly in the H15–H1–H7–G204 well block and surrounding areas where the TDS content of wells is >40 g L^{-1} (maximum 241 g L^{-1}, Well H15). The area with the next-highest TDS values is the G201–G80–H5 well block, with TDS contents of >20 g L^{-1} (Figure 9a). The TDS high-value areas are distributed mainly in the fan delta front, with TDS content decreasing along the source direction, i.e., the nearer the depression center, the lower the TDS content. The fan delta front subfacies of the Upper Urho Formation comprise three microfacies: subsea river channel, river mouth dam, and sheet sand. These are developed along the source direction, with decreasing clay content. Muddy shale and argillaceous siltstone in the submarine river channel form the caprock, which enhances the sealing of the reservoir and promotes the concentration of oilfield water, with a resulting high TDS content. The delta barrier and sheet sand are strongly influenced by the external environment, having experienced more active hydrodynamic conditions. The TDS value of oilfield water in these microfacies is usually low. Thus, the sedimentary facies and source direction have a major effect on the chemical characteristics of oilfield water.

The r_{Na}/r_{Cl} ratio is distributed with a zonal pattern in map view (Figure 9b). Areas with a high r_{Na}/r_{Cl} ratio also have high TDS contents, while low-ratio areas are distributed mainly in the G10–L2–L7–L4–G83 and H5–H7–H1–Z7 well blocks (Figure 9b). The $r_{SO_4} \times 100/r_{Cl}$ ratio is generally low, and the higher-value area in the M9–J7 well block is strongly correlated with the low-TDS and the high-r_{Na}/r_{Cl} areas (Figure 9c). The high-porosity, high-TDS, low- r_{Na}/r_{Cl}, and low- $r_{SO_4} \times 100/r_{Cl}$ areas are consistent (Figure 9d). According to oil and gas exploration data of the Xinjiang Oilfield Exploration and Development Research Institute (September 2021), 34 layers in 24 wells contain industrial-grade oil in the western periphery of the Mahu Sag. Eighteen layers in 15 wells are of the Upper Urho Formation, eight layers in eight wells are of the Lower Urho Formation, and two layers in one well are of the Xiazijie Formation (Table 4). These wells are distributed in areas with relatively high TDS, low r_{Na}/r_{Cl}, and low $r_{SO_4} \times 100/r_{Cl}$ values, especially high-productivity wells such as H014, H015, H18, H22, H27, and H017, which have TDS contents of >20 g L^{-1}, r_{Na}/r_{Cl} ratios of <0.75, and $r_{SO_4} \times 100/r_{Cl}$ ratios of <5. These high-productivity wells are distributed in the fan delta front (Figure 9a–d). Reservoirs in this sedimentary environment are usually widely distributed and well sorted, with thick sand bodies and high exploration potential. These results demonstrate the importance of the chemical properties of oilfield water in petroleum exploration and provide a reference for Permian oil and gas development in the western periphery of the Mahu Sag.

Table 4. Oil and gas exploration results for the western periphery of the Mahu Sag.

No.	Well	Formation	Deep (m)	Oil Production (m^3/day)	Gas Production (10^4 m^3/day)
1	H014	P_3w_2	3737~3844	138.29	0.86
		P_3w_1	3681~3702	7.40	
2	H015	P_3w_2	3614~3649	26.20	0.18
		T_1b	3496~3551	6.20	
3	H10	P_3w_2	3570~3573	6.30	
4	H11	P_3w	3364~3396	8.70	
		T_1b	3230~3264	8.00	
5	H14	P_2w	4100~4179	18.80	

Table 4. *Cont.*

No.	Well	Formation	Deep (m)	Oil Production (m^3/day)	Gas Production (10^4 m^3/day)
6	H18	P_3w_1	3741~3755	6.85	
		P_3w_2	3642~3682	21.70	0.33
7	H21	P_2w	3578~3652	7.30	
8	H22	P_2w	3586~3668	25.60	
9	H23	P_3w_1	4283~4316	11.62	
10	H24	P_3w_2	3182~3205	16.64	
11	H27	P_2w	3281~3285	10.20	0.68
12	H29	P_3w_2	3242~3245	22.20	0.23
13	Z7	P_2w	4466~4563	18.62	
14	H016	P_2w	3724~3748	5.70	
		P_3w_{21}	3563~3568.5	12.30	
		T_1b	3454~3495	12.50	
15	H017	P_2w	3624.5~3646.5	20.50	
		P_3w_{12}	3537~3554	36.20	
		P_3w_{11}	3494~3505.5	27.80	
16	H018	P_2w	3672~3684	6.20	
		P_3w_{12}	3640~3658	7.40	
17	H402	T_1b_2	3411~3434	9.40	
18	G891	P_3w	3072~3078	6.00	
19	G204	P_3w_{22}	3575~3584	6.50	
20	G205	P_2x	4339~4352	22.20	
			4268~4286	12.40	
21	L47	P_3w_2	3225~3254	6.90	0.85
22	M901	T_1b	3521.5~3529	6.50	
23	G811	T_1b	3220~3227	8.80	
24	J225	P_3w	3461~3489	6.60	

7. Conclusions

Permian oilfield water in the western periphery of the Mahu Sag is characterized by high TDS, Cl^-, (Na^+ + K^+), HCO_3^-, and Ca^{2+} concentrations, and is mainly $CaCl_2$-type water. The Upper and Lower Urho formations have low r_{Na}/r_{Cl}, $r_{SO_4} \times 100/r_{Cl}$, $(r_{HCO_3+CO_3})/r_{Ca}$, and r_{Mg}/r_{Ca} ratios, reflecting a regional zone of hydrodynamic stagnation where reservoirs are well sealed and conducive to the preservation of oil and gas. The $r_{SO_4} \times 100/r_{Cl}$ ratios of the Fengcheng and Xiazijie formations are relatively low, while the r_{Na}/r_{Cl}, $(r_{HCO_3+CO_3})/r_{Ca}$, and r_{Mg}/r_{Ca} ratios are much higher than those of the Jiamuhe and Upper and Lower Urho formations. This indicates a decreasing content of secondary pores in the reservoirs, with a weak concentration of oilfield water. Reservoir sealing is also weaker, and oil and gas preservation conditions are not as strong as in the Jiamuhe, Upper, and Lower Urho formations.

The genesis of the Permian oilfield water is complex and is mainly influenced by tectonic activity, paleoclimate, and water–rock interaction. Volcanic activity generated plentiful alkali and alkaline–earth metal ions. A hot, dry paleoclimate produced a saline alkaline lake sedimentary environment. Both factors provided rich material for oilfield water sources. Regarding water–rock interaction, the Jiamuhe and Upper and Lower Urho formations were affected by the sodic feldspathization of Ca-feldspars; the Fengcheng Formation was influenced by the dissolution of carbonate rocks and hydrocarbon expulsion from source rocks; the Xiazijie Formation was affected by the sodic feldspathization of Ca-feldspars and salt rock dissolution while also being controlled by the complex Permian fault system.

Sodic feldspathization and the dissolution of Ca-feldspars were important during the diagenesis of the western periphery of the Mahu Sag, having a major effect on reservoir

physical properties. Secondary pores generated by dissolution resulted in improved reservoir quality. The relationship between the chemical characteristics of oilfield water and the distribution of high-yield petroleum wells indicates that high-TDS, $CaCl_2$-type oilfield water areas with low r_{Na}/r_{Cl}, $r_{SO_4} \times 100/r_{Cl}$, $(r_{HCO_3+CO_3})/r_{Ca}$, and the r_{Mg}/r_{Ca} ratios are relatively conducive to the preservation of oil and gas.

Author Contributions: Conceptualization, R.Z.; methodology, A.J.; validation, Z.L.; formal analysis, S.Z.; investigation, J.L.; resources, J.J.; data curation, S.Z.; writing—original draft preparation, J.L.; writing—review and editing, A.J.; visualization, R.Z.; supervision, R.Z.; project administration, J.J.; funding acquisition, Z.L. All authors have read and agreed to the published version of the manuscript.

Funding: This research was funded by the Foundation of "National Science and Technology major projects (No. 2011ZX05002-006-003HZ)".

Data Availability Statement: Not applicable.

Conflicts of Interest: The authors declare no conflict of interest.

References

1. Lewan, M.D. Experiments on the role of water in petroleum formation. *Geochim. Cosmochim. Acta* **1997**, *61*, 3691–3723. [CrossRef]
2. Pan, C.C.; Geng, A.S.; Zhong, N.N.; Liu, J.Z.; Yu, L.P. Kerogen pyrolysis in the presence and absence of water and minerals: Amounts and compositions of bitumen and liquid hydrocarbons. *Fuel* **2009**, *88*, 909–919. [CrossRef]
3. Wei, L.; Gao, Z.Y.; Mastalerz, M.; Schimmelmann, A.; Gao, L.; Wang, X.; Liu, X.X.; Wang, Y.; Qiu, Z. Influence of water hydrogen on the hydrogen stable isotope ratio of methane at low versus high temperatures of methanogenesis. *Org. Geochem.* **2019**, *128*, 137–147. [CrossRef]
4. Bachu, S.; Underschultz, J.R. Hydrogeology of formation waters, northeastern Alberta basin. *AAPG Bull.* **1993**, *77*, 1745–1768.
5. Verweij, J.M. *Hydrocarbon Migration Systems Analysis*; Elsevier: Amsterdam, The Netherlands, 1993.
6. Mccaffrey, M.A.; Lazar, B.H.D.H.; Holland, H.D. The evaporation path of seawater and the coprecipitation of Br^- and K^+ with halite. *J. Sediment. Res.* **1987**, *57*, 928–937.
7. Davisson, M.L.; Criss, R.E. Na-Ca-Cl relations in basinal fluids. *Geochim. Cosmochim. Acta* **1996**, *60*, 2743–2752. [CrossRef]
8. Worden, R.H.; Coleman, M.L.; Matray, J.M. Basin scale evolution of formation waters: A diagenetic and formation water study of the Triassic Chaunoy Formation, Paris Basin. *Geochim. Cosmochim. Acta* **1999**, *63*, 2513–2528. [CrossRef]
9. Grassi, S.; Cortecci, G.; Squarci, P. Groundwater resource degradation in coastal plains: The example of the Cecina area (Tuscany–Central Italy). *Appl. Geochem.* **2007**, *22*, 2273–2289. [CrossRef]
10. Li, Q.G.; Ju, Y.W.; Lu, W.Q.; Wang, G.C.; Neupane, B.; Sun, Y. Water-rock interaction and methanogenesis in formation water in the southeast Huaibei coalfield, China. *Mar. Pet. Geol.* **2016**, *77*, 435–447. [CrossRef]
11. Xie, X.N.; Jiao, J.J.; Cheng, J.M. Regional variation of formation water chemistry and diagenesis reaction in underpressured system: Example from Shiwu depression of Songliao basin, NE China. *J. Geochem. Explor.* **2003**, *78*, 585–590.
12. Al-Hajeri, M.M.; Bowden, S.A. Application of formation water geochemistry to assess seal integrity of the Gotnia Formation, Kuwait. *Arab. J. Geosci.* **2017**, *10*, 56. [CrossRef]
13. Cheng, J.M.; McIntosh, J.C.; Xie, X.N.; Jiao, J.J. Hydrochemistry of formation water with implication to diagenetic reactions in Sanzhao depression and Qijia-gulong depression of Songliao Basin, China. *J. Geochem. Explor.* **2006**, *88*, 86–90. [CrossRef]
14. Wang, Q.M.; Hu, Q.H.; Larsen, C.; Zhao, C.; Sun, M.D.; Zhang, Y.X.; Zhang, T. Microfracture-pore structure characterization and water-rock interaction in three lithofacies of the Lower Eagle Ford Formation. *Eng. Geol.* **2021**, *292*, 106276. [CrossRef]
15. Zhang, C.M.; Song, X.M.; Wang, X.J.; Wang, X.L.; Zhao, K.; Shuang, Q.; Li, S.H. Origin and depositional characteristics of supported conglomerates. *Pet. Explor. Dev.* **2020**, *47*, 292–305. [CrossRef]
16. Ma, H.N.; Tang, C.; Qiu, Z.Y.; Xiang, J.L. Reservoir Characteristics and Main Controlling Factors of Lower Wuerhe Formation in Madong Slope Belt of Mahu Sag. *Fresenius Environ. Bull.* **2021**, *30*, 11287–11296.
17. Jia, H.B.; Ji, H.C.; Wang, L.S.; Gao, Y.; Li, X.W.; Zhou, H. Reservoir quality variations within a conglomeratic fan-delta system in the Mahu sag, northwestern Junggar Basin: Characteristics and controlling factors. *J. Pet. Sci. Eng.* **2017**, *152*, 165–181. [CrossRef]
18. Yu, K.H.; Cao, Y.C.; Qiu, L.W.; Sun, P.P.; Yang, Y.Q.; Qu, C.S.; Lei, D.W.; Jia, X.Y.; Wan, M.; Zhang, Z.J. Unconformity-controlled dissolution contributes to reservoirs in the carbonate-rich Permian Fengcheng Formation, northwestern Junggar Basin, China. *Carbonates Evaporites* **2020**, *35*, 26. [CrossRef]
19. Feng, C.; Ma, M.Z.; He, W.J.; Li, T.; Wu, Q.Y.; Zhang, Z.X.; Zhao, H.Y. Paleoenvironmental changes of source rocks from the Carboniferous to Permian sediments of the Mahu Sag, Junggar Basin, China. *Geosystem Eng.* **2020**, *23*, 276–286. [CrossRef]
20. Xiang, B.L.; Li, E.T.; Gao, X.W.; Wang, M.; Wang, Y.; Xu, H.; Huang, P.; Yu, S.; Liu, J.Z.; Zou, Y.R.; et al. Petroleum generation kinetics for Permian lacustrine source rocks in the Junggar Basin, NW China. *Org. Geochem.* **2016**, *98*, 1–17. [CrossRef]
21. Liang, Y.Y.; Zhang, Y.Y.; Chen, S.; Guo, Z.J.; Tang, W.B. Controls of a strike-slip fault system on the tectonic inversion of the Mahu Sag at the northwestern margin of the Junggar Basin, NW China. *J. Asian Earth Sci.* **2020**, *198*, 104229. [CrossRef]

22. Zhang, C.M.; Yin, T.J.; Tang, Y.; Guo, X.G.; Zhao, K.; Pan, J.; Chen, M.L. Advances in sedimentological reservoir research in Mahu sag and northwest margin ofJunggar Basin. *J. Palaeogeogr.* **2020**, *22*, 129–146.
23. Lian, Y.C. Geologic Structure and Tectonic Evolution of the Karamay-Baikouquan Overthrust Belt at the Northwestern Margin of Junggar Basin. Master's Thesis, China University of Geosciences, Beijing, China, 2016.
24. Imin, A.; Zha, M.; Ding, X.J.; Bian, B.L.; Liu, Y.; Zheng, M.L.; Han, C. Identification of a Permian foreland basin in the western Junggar Basin (NW China) and its impact on hydrocarbon accumulation. *J. Pet. Sci. Eng.* **2020**, *187*, 106810. [CrossRef]
25. *SY/T 5523-2016*; Method for Analysis of Oilfiled Water. Petroleum Industry Press: Beijng, China, 2016.
26. Cheng, Z.H.; Wang, S.N.; Wang, L.; Cha, M. Characteristics of formation water chemical fields and its petroleum significance of the Neogene in Dongying Sag, Shandong Province. *J. Palaeogeogr.* **2012**, *14*, 685–693.
27. Akstinat, M. Chemical and physicochemical properties of formation waters of the oil and gas industry. *J. Hydrol.* **2019**, *578*, 124011. [CrossRef]
28. Guseva, N.V.; Kopylova, Y.G.; Oidup, C.K.; Arakchaa, K.D.; Rychkova, K.M.; Khvashchevskaya, A.A.; Ayunova, O.D. Formation of the chemical composition of brackish and brine groundwater in the Tuva depression and surrounding areas. *Russ. Geol. Geophys.* **2018**, *59*, 135–143. [CrossRef]
29. Chen, J.; Liu, D.Y.; Hou, X.L.; Fan, Y.K.; Jia, W.L.; Peng, P.A.; Zhang, B.S.; Xiao, Z.Y. Origin and evolution of oilfield waters in the Tazhong oilfield, Tarim Basin, China, and their re-lationship to multiple hydrocarbon charging events. *Mar. Pet. Geol.* **2018**, *98*, 554–568. [CrossRef]
30. Collins, A.G. *Geochemistry of Oilfield Waters*; Elsevier: Amsterdam, The Netherlands, 1975.
31. Surin, B.A.; Wang, C.Y. *Oilfield Waters in Natural Water Systems*; Petroleum Industry Press: Beijng, China, 1956.
32. Zhang, S.W.; Zhang, L.Y.; Bao, Y.S.; Li, X.Y.; Liu, Q.; Li, J.Y.; Yin, Y.; Zhu, R.F.; Zhang, S.C. Formation fluid characteristics and hydrocarbon accumulation in the Dongying sag, Shengli Oilfield. *Pet. Explor. Dev.* **2012**, *39*, 423–435. [CrossRef]
33. Xie, X.N.; Fan, Z.H.; Liu, X.F.; Lu, Y.C. Geochemistry of formation water and its implication on over pressured fluid flow in the Dongying Depression of the Bohaiwan Basin, China. *J. Geochem. Explor.* **2006**, *89*, 432–435. [CrossRef]
34. Çelik, M.; Sari, A. Geochemistry of formation waters from upper cretaceous calcareous rocks of Southeast Turkey. *J. Geol. Soc. India* **2002**, *59*, 419–430.
35. Tao, H.F.; Qu, Y.Q.; Wu, T.; Liu, B.B. Oilfield water and favorable petroleum exploration targets for the triassic baikouquan formation in the slope of Mahu Sag, junggar basin. *Geofluids* **2021**, *2021*, 6699489. [CrossRef]
36. Yang, C.L.; Xie, Z.Y.; Pei, S.Q.; Guo, J.Y.; Zhang, L.; Dong, C.Y.; Hao, A.S.; Yang, C.X.; Liu, Z.X. Chemical characteristics of Middle Permian formation water and hydrocarbon preservation conditions in Northwest Sichuan. In *IOP Conference Series: Earth and Environmental Science*; IOP Publishing: Bristol, UK, 2020; Volume 600, p. 012041.
37. Tang, W.B.; Zhang, Y.Y.; Pe-Piper, G.; Piper, D.J.; Guo, Z.J.; Li, W. Permian rifting processes in the NW Junggar Basin, China: Implications for the post-accretionary successor basins. *Gondwana Res.* **2021**, *98*, 107–124. [CrossRef]
38. Tang, W.B.; Zhang, Y.Y.; Pe-Piper, G.; Piper, D.J.; Guo, Z.J.; Li, W. Permian to early Triassic tectono-sedimentary evolution of the Mahu sag, Junggar Basin, western China: Sedimentological implications of the transition from rifting to tectonic inversion. *Mar. Pet. Geol.* **2021**, *123*, 104730. [CrossRef]
39. Tang, W.; Zhang, Y.; Pe-Piper, G.; Piper, D.J.W.; Guo, Z.; Li, W. Soft-sediment deformation structures in alkaline lake deposits of Lower Permian Fengcheng Formation, Junggar Basin, NW China: Implications for syn-sedimentary tectonic activity. *Sediment. Geol.* **2020**, *406*, 105719. [CrossRef]
40. Zhang, Z.J.; Yuan, X.J.; Wang, M.S.; Zhou, C.M.; Tang, Y.; Chen, X.Y.; Lin, M.J.; Cheng, D.W. Alkaline-lacustrine deposition and paleoenvironmental evolution in Permian Fengcheng Formation at the Mahu sag, Junggar Basin, NW China. *Pet. Explor. Dev.* **2018**, *45*, 1036–1049. [CrossRef]
41. Cao, J.; Zhang, Y.J.; Hu, W.X.; Yao, S.P.; Wang, X.L.; Zhang, Y.Q.; Tang, Y. The Permian hybrid petroleum system in the northwest margin of the Junggar Basin, northwest China. *Mar. Pet. Geol.* **2005**, *22*, 331–349. [CrossRef]
42. Chen, S.P.; Zhang, Y.W.; Tang, L.J.; Bai, G.P. Tectonic Evolution of the Junggar Foreland Basin in the Late Carboniferous-Permian. *Acta Geol. Sin. Engl. Ed.* **2001**, *75*, 398–408.
43. Chen, Y.B.; Cheng, X.G.; Zhang, H.; Li, C.Y.; Ma, Y.P.; Wang, G.D. Fault characteristics and control on hydrocarbon accumulation of middle-shallow layers in the slope zone of Mahu sag, Junggar Basin, NW China. *Pet. Explor. Dev.* **2018**, *45*, 1050–1060. [CrossRef]
44. Li, H.X.; Cai, C.F. Origin and evolution of formation water from the Ordovician carbonate reservoir in the Tazhong area, Tarim Basin, NW China. *J. Pet. Sci. Eng.* **2017**, *148*, 103–114. [CrossRef]
45. Yang, L.J.; Hou, D.J.; Chen, X.D. Chemical characteristics and geological significance of Palaeogene formation water in central Xihu Depression, East China Sea Basin. *Nat. Gas Geosci.* **2018**, *29*, 559–571.
46. An, T.; Yu, B.S.; Wang, Y.S.; Ruan, Z.; Meng, W.; Feng, Y.L. Water-rock interactions and origin of formation water in the Bohai Bay Basin: A case study of the Cenozoic Formation in Bonan Sag. *Interpretation* **2021**, *9*, T475–T493. [CrossRef]
47. Wang, J.; Lou, Z.H.; Zhu, R.; Jin, A.M. The migration of hydrocarbons: A case from the Shahejie formation of the Wenliu area of Bohai Bay Basin, China. *Pet. Sci. Technol.* **2019**, *37*, 38–49. [CrossRef]
48. Bozau, E.; Sattler, C.D.; Berk, W. Hydrogeochemical classification of deep formation waters. *Appl. Geochem.* **2015**, *52*, 23–30. [CrossRef]

49. Wu, J.B.; Yang, S.L.; Gan, B.W.; Cao, Y.S.; Zhou, W.; Kou, G.; Wang, Z.Q.; Li, Q.; Dong, W.G.; Zhao, B.B. Pore Structure and Movable Fluid Characteristics of Typical Sedimentary Lithofacies in a Tight Conglomerate Reservoir, Mahu Sag, Northwest China. *ACS Omega* **2021**, *6*, 23243–23261. [CrossRef] [PubMed]
50. Li, X.; Zhou, W.; Zhou, Q.; Wu, R.B.; Yang, Z.B.; Wang, Y.T.; Peng, X.H.; Liang, T. Study on Permian Sedimentary Environment and Reservoir Characteristics in Mahu Sag, Junggar Basin, China. *Fresenius Environ. Bull.* **2021**, *30*, 8886–8898.
51. Kong, R.S. Research on the Mechanism of Low-Salinity Waterflooding. Master's Thesis, China University of Geosciences, Beijing, China, 2017. (in Chinese).
52. Birkle, P.; García, B.M.; Padrón, C.M.M.; Eglington, B.M. Origin and evolution of formation water at the Jujo–Tecominoacán oil reservoir, Gulf of Mexico. Part 2: Isotopic and field-production evidence for fluid connectivity. *Appl. Geochem.* **2009**, *24*, 555–573. [CrossRef]
53. Birkle, P.; García, B.M.; Padrón, C.M.M. Origin and evolution of formation water at the Jujo–Tecominoacán oil reservoir, Gulf of Mexico. Part 1: Chemical evolution and water–rock interaction. *Appl. Geochem.* **2009**, *24*, 543–554. [CrossRef]